International Journal of Electrochemical Science 18 (2023) 100288

Contents lists available at ScienceDirect

International Journal of Electrochemical Science

journal homepage: www.editorialmanager.com/ijoes

Measuring the ionic conductivity of solid polymer electrolyte powders

Ana Laura G. Biancolli [a,b], Anastasiia Konovalova [a], Elisabete I. Santiago [b], Steven Holdcroft [a,*]

[a] Holdcroft Research Group, Department of Chemistry, Simon Fraser University, 8888 University Drive, Burnaby, BC, Canada V5A 1S6
[b] Nuclear and Energy Research Institute, IPEN/CNEN, 05508-000 São Paulo, Brazil

ARTICLE INFO

Keywords:
Ionic conductivity
Ion-exchange polymer powders
Through-plane ion conductivity
Solid polymer electrolyte

ABSTRACT

Ex-situ characterization of solid polymer electrolytes plays an important role in their development as materials for energy applications, with ionic conductivity being a crucial parameter to quantify. Conventional measurements of ionic conductivity often require the formation of a free-standing polymer film which in many instances is difficult to fabricate, thus there may be a need to quantify their ionic conductivity in powder form. In this work, we present a practical and reproducible method for measuring the ionic conductivity of solid polymer electrolytes (SPEs) in their powder form. By using a modified configuration of a through-plane cell, demonstrated with both a proton conducting- and an anion conducting-solid polymer electrolyte powder (SPEP), we are able to obtain ionic conductivity values under variable conditions in order to explore the influence of external parameters on the ionic conductivity of powders. Two types of SPEs in insoluble powder form were employed in this work: (1) a proton-exchange material (SPEP-H^+) based on a hyperbranched, sulfo-phenylated poly(phenylene) SPEP (HB-sPPT-H^+), with measured ionic conductivity of ~ 210 mS cm^{-1} at 80 °C and 95 % of relative humidity (RH); (2) an anion-exchange conducting polymer in its chloride form (SPEP-Cl^-), consisting of a radiation-grafted ultra-high density polyethylene insoluble SPEP containing covalently-bonded benzyltrimethylammonium (BTMA) head-groups, with measured ionic conductivity of ~ 53 mS cm^{-1} at 80 °C and 95 % RH.

1. Introduction

A rise in global temperature calls for the quick and effective development of renewable energy grids [1,2]. As an integral part of energy networks, electrochemical energy conversion devices such as fuel cells and electrolyzers have received increased attention over the past two decades [3,4]. Components of these systems include polymer electrolyte membranes and catalyst layers, which have been actively investigated in search of cheaper and more sustainable options [5–7]. As an alternative to the widely used commercial perfluorosulfonic acid membranes, hydrocarbon-based solid polymer electrolytes are being extensively researched [8–11]. Emerging polymers require a comprehensive set of characterizations to determine compatibility with prospective applications. Especially important is the determination of the ionic conductivity of materials as this property exerts a profound influence on the performance of electrochemical energy conversion devices. Characterization of ionic transport phenomena is primarily performed on the thin membrane form of the polymer electrolytes. However, not all newly synthesized materials can be fabricated into free-standing films. Moreover, solid polymer electrolytes in their powder form are gaining attention as additives to catalyst layers to enhance the transport of ions [12–15]. A technique capable of measuring the ionic conductivity of powder polymers is thus warranted as this will assist in fine-tuning synthetic routes of ionic polymers during the early stages of the material development.

There are several areas of research that typically require the investigation of conductivity of powders. The first field concerns solid oxide fuel cells (SOFC), which utilize pressed pellets of the electrolyte that are subsequently sintered. Upon sputtering metal on the pellet's surface, ionic conductivity can be measured using electrochemical impedance spectroscopy (EIS) [16]. A second area is the evaluation of the electrical conductivity of carbons for a multitude of applications. Typically, a carbon powder is compressed between two metal rods inside a small electrically insulating cylinder and the electrical conductivity is evaluated via EIS [17]. The conductivity of powders is also explored in one of the largest fields of energy research, solid-state batteries. In this case, for example, Li^+ ion conducting composites (e.g., sulfide or carbonate-based) are studied using a technique similar to the one used in SOFC research. The two-point probe EIS measurement, utilizing ion-blocking or electron-blocking electrodes, is a simple method for determining the material's conductivity in a hard-pressed pellet form

* Corresponding author.
E-mail address: holdcrof@sfu.ca (S. Holdcroft).

https://doi.org/10.1016/j.ijoes.2023.100288
Received 31 May 2023; Received in revised form 10 July 2023; Accepted 19 July 2023
Available online 20 July 2023

[18,19]. These assemblies served as inspiration to our research group to utilize physical confinement and compressed pellet to evaluate the ionic conductivity of solid polymer electrolytes in their powder form.

In this work, we present a practical and reproducible method of measuring the ionic conductivity of solid polymer electrolytes (SPE) in their insoluble powder form using Scribner Associates MTS-740 equipment and its through-plane conductivity cell. This method allows to record the resistance of SPE powders as a function of relative humidity and temperature, and above the boiling point of water by application of back pressure. The latter is especially relevant to the emerging field of high-temperature alkaline fuel cells [20–22]. Additionally, we compare conductivity data to that obtained using a conventional through-plane conductivity cell, where the polymer powder is compressed between two stainless steel rods tipped with platinum electrodes.

2. Experimental

2.1. Ion-conducting solid polymer electrolyte (SPE) powders

Two types of SPEs in insoluble powder form were employed in this work: (1) a proton-exchange solid polymer electrolyte powder **(SPEP-H^+)** based on a hyperbranched, sulfo-phenylated poly(phenylene) solid polymer electrolyte powder (HB-sPPT-H^+) possessing an ion-exchange capacity of 2.76 ± 0.1 mmol g^{-1} (Fig. S1a). The material is insoluble in common laboratory polar protic solvents and was provided in its ball-milled form. The preparation and characterization of this material is reported elsewhere [14]. **(2)** An anion-exchange solid polymer electrolyte powder in its chloride form (**SPEP-Cl^-**), consisting of a radiation-grafted ultra high-density polyethylene insoluble solid polymer electrolyte powder containing covalently-bonded benzyltrimethylammonium (BTMA) head-groups (Fig. S1b). This material was synthesized by following the procedure reported in [13], but using a polyethylene-based backbone instead of ethylene tetrafluoroethylene (unpublished results). The measured ion-exchange capacity was 2.55 ± 0.1 mmol g^{-1}. Both materials have been previously introduced to catalyst layers of fuel cells in their powder form to improve the ion conductivity of the catalyst layer.

2.2. Dynamic Vapor Sorption (DVS)

Dynamic Vapor Sorption (DVS) measurements were performed on a DVS Adventure humidity chamber and Ultrabalance (Surface Measurement Systems Ltd., UK). SPE powder was dried in a vacuum oven (80 °C, 17 h) and the dry mass of the material was recorded in the DVS instrument at the initial step. The humidity was controlled by a source of deionized water delivered under nitrogen gas flow at a volumetric flow rate of 200 standard cubic centimeters per minute (sccm). The maximum accessible relative humidity (RH) was limited by the machine at elevated temperatures. The experiment was conducted in two stages. In the first stage, samples were held at a constant temperature of 80 °C and absorption/desorption curves were recorded under a stepwise increase of relative humidity in the 0–74 % RH range. As for the second stage, relative humidity was fixed at a level of 76 ± 3 % and the temperature was increased from 40 to 80 °C in 10 °C steps. Water uptake, *WU* [%], was calculated according to Eq. (1). Additionally, the hydration number, λ – the number of water molecules per ion pair, was calculated from the ratio of moles of water, $n_{H2O/mol}$, per dry mass of polymer, m_{dry} [g], with respect to ion exchange capacity, *IEC* [mmol g^{-1}], as shown by Eq. (2).

$$WU = \frac{m_{wet} - m_{dry}}{m_{dry}} \quad (1)$$

$$\lambda = \frac{n_{H_2O}}{IEC \bullet m_{dry}} \quad (2)$$

2.3. Thermal gravimetric analysis (TGA)

Thermal degradation data of ~ 10 mg of powder polymer samples was obtained using a thermogravimetric analyzer PerkinElmer TGA 4000. The samples were heated under N_2 at 10 °C min^{-1} from 30 °C up to 700 °C.

2.4. Through-plane conductivity

Conductivity measurements of SPEs in powder form were performed using two experimental setups: I) a commonly found method in the literature [23–25], which uses a conventional in-house fabricated glass cell placed inside an environmental chamber with temperature and relative humidity control coupled to a Solartron Analytical 1260 Impedance Analyzer; II) a novel methodology using a Scribner Associates Membrane Test System MTS-740 coupled to a Solartron Analytical 1260 Impedance Analyzer.

2.4.1. Experimental setup I

Through-plane proton (H^+) or anion (Cl^-) conductivities were measured by compressing a given quantity of polymer powder between two stainless steel rods tipped with Pt disks electrodes inside a 0.58 cm diameter glass tube as illustrated in Fig. 1. The thickness of the circular pellet of powder (approximately 2–3 mm) was accurately measured with a digital caliper following the experiment. The in-house fabricated glass cell was kept under compression in a clamp during the measurement to ensure sufficient electric contact between the components. The impedance of the cell was measured over the frequency range of 10 MHz to 100 Hz at 100 mV amplitude. The assembly was equilibrated at 80 °C at each relative humidity step in an environmental chamber (SH-241, ESPEC North America Inc.) for 24 h. For conductivity-temperature dependence measurements, the cell was equilibrated at 95 % RH for 24 h and then 2 h for each temperature at the same RH. To obtain SPEP-H^+ conductivities, it was necessary to add a drop of water to the sample prior to equilibration in the chamber, thus this measurement was considered as being under "fully humidified" conditions. The resulting spectra were corrected by the respective shorted cells' inductance and fitted using a Randles simplified equivalent circuit to obtain the ionic resistance [26]. The ionic conductivity σ [S cm^{-1}] was calculated using Eq. (3), where *L* [cm] is the thickness of the pellet, *A* [cm^2] is its surface area, and *R* [Ohm] is the measured resistance.

$$\sigma = \frac{L}{R \times A} \quad (3)$$

2.4.2. Experimental setup II

The 740 Membrane Test System (MTS-740) from Scribner Associates and its through-plane conductivity cell head were used for measuring the ionic conductivity of SPEP-H^+ and SPEP-Cl^- materials. Two tools were manufactured in-house to assist the through-plane measurements in the MTS-740 equipment: 1) an electrode-sized mold for compacting powder under pressure (Fig. 2), and 2) two polyamide lateral shields, as shown in Fig. 3a, which were fixed to the cell by the screw-compressor clamp shown in Fig. 3b. Lateral shields were installed on the sides of the MTS-740 cell to prevent possible dispersion of the powder within the humidity chamber due to the loss of the mechanical integrity of the

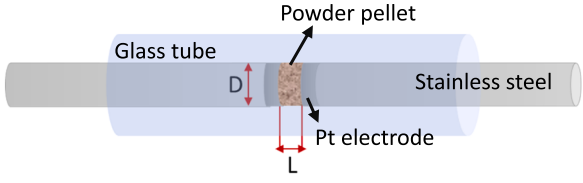

Fig. 1. Scheme of a conventional through-plane conductivity glass cell with labeled components.

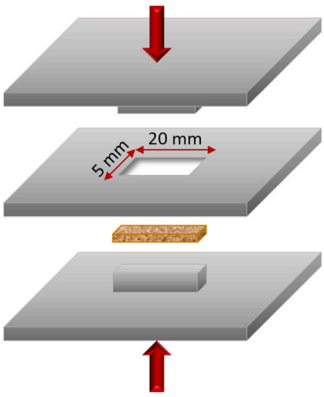

Fig. 2. Schematic image of the pellet preparation process using an electrode-sized mold.

pellet (Fig. 3c–f). Pellets with a fixed area of 20 × 5 mm^2 were prepared by using the custom-made mold and a hydraulic press Carver, Inc. Model 3851-0. The free-standing pellet was placed into the MTS-740 through-plane cell ensuring that it would be in contact with all four electrodes. A compression head dial indicator was installed to measure the pressure applied to the electrodes. The compression head of the cell was rotated three times, resulting in 119 PSI of compression. The hydrated thickness of the samples (0.5–1.5 mm) was measured by a caliper while the material was inside the cell and after completing the experiment. The ionic resistances of SPE powder pellets were collected during water absorption (from 50 % to 95 % RH, in 5–10 % steps) and desorption (from 95 % to 50 % RH, 5–10 % steps) at 80 °C, and at fixed 95 % RH and varying temperature from 40 to 80 °C and 80 to 40 °C, in 10 °C steps. The system provides fully automated control of the sample temperature, dew point, and therefore relative humidity. The RH is controlled by using a wet-dry gas mixing humidification system and a flow of 500 sccm of N_2 (99.998 %) was applied. The equilibrium time for individual steps was 4 h, with measurements being taken every 30 min in the frequency range of 10 MHz to 1 Hz at 10 mV of amplitude. Eq. (3) was used to calculate the through-plane conductivity, where L [cm] is the thickness of the humidified SPE pellet, A [cm^2] is the Pt electrode surface area (0.5 cm^2), and R [Ohm] is the measured resistance.

3. Results and discussion

3.1. Water uptake and thermal stability of SPE powders

The ionic conductivity of SPEs is highly dependent on their water content [27–29], hence, it is necessary to evaluate water absorption and desorption in order to understand ion conduction within the materials. Water uptake was evaluated by DVS under dependencies of relative humidity and temperature. Firstly, the humidity dependence was recorded under a constant temperature of 80 °C, up to the maximum RH allowed by the equipment. Representative isothermal water absorption and desorption curves for the SPEs are shown in Fig. 4. As can be seen from the absorption plot, water uptake of both anionic and cationic materials increases with the increasing RH, reaching 41 wt% for SPEP-H^+ and 21 wt% for SPEP-Cl^- at 73 % RH. The hydration number of the SPE powders under the same conditions is 28 for SPEP-H^+ and 12 for SPEP-Cl^-. The water absorption behavior of the materials is linear, with SPEP-H^+ being prone to a higher water uptake. However, as determined by the desorption isotherms, hysteresis is observed for the proton-exchange SPE material. This suggests a large distribution of pore sizes throughout the material. Large pores are connected to narrow pores so the desorption of water from a larger pore is restricted by the prioritized desorption of a smaller pore. In contrast, SPEP-Cl^- exhibits negligible hysteresis. This difference in behavior is related to the intrinsic properties of each SPE, which is determined by the material's morphology and arrangement of hydrophilic and hydrophobic domains. In the case of SPEP-Cl^-, the material has a hydrophobic polyethylene backbone bearing grafted side chains that are responsible for conducting anions. Contrarily, the SPEP-H^+ is an ionene, which incorporates cations directly along its polymer backbone. In this context, a hypothesis is that the water penetrates deeper into the interchains of the SPEP-H^+, than in the SPEP-Cl^- in which the water would be more surficial along pore-walls. The different distribution of water in the materials might be responsible for the distinct shapes of the water uptake curves.

Secondly, the water uptake-temperature dependence was evaluated

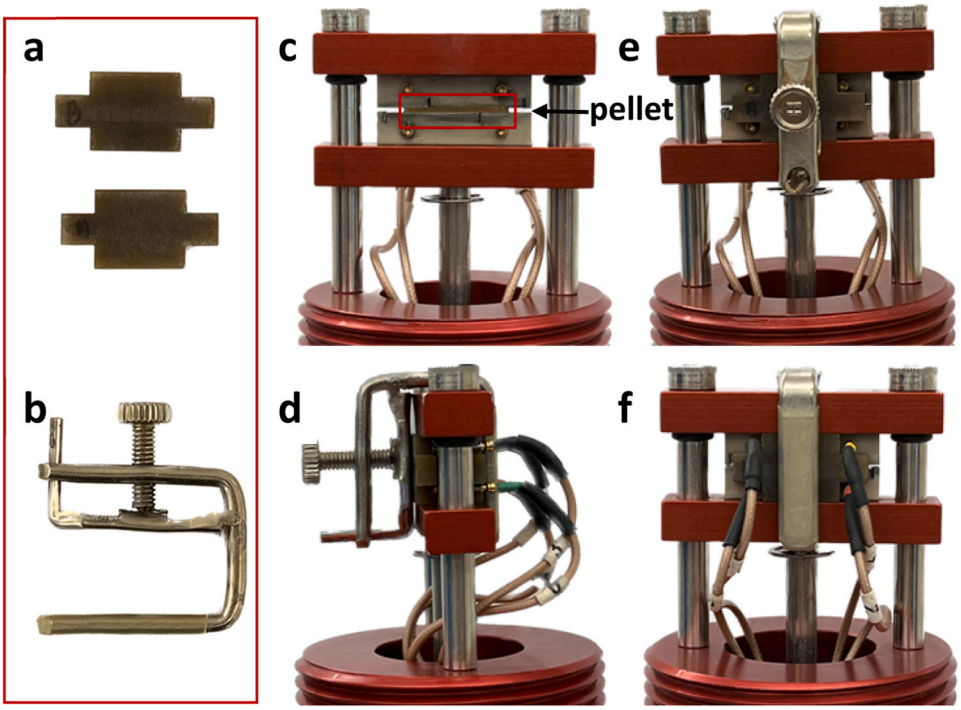

Fig. 3. MTS-740 through-plane conductivity cell with added modifications: a) polyamide lateral shields; b) brass clamp; c) frontal view of the electrode assembly with a solid polymer electrolyte (SPE) powder pellet; d) side view of the electrode assembly with the polyamide lateral shields and the clamp installed; e) rear view of the cell with polyamide lateral shields clamped to the electrode assembly; f) front view of the electrode assembly with the polyamide lateral shields and the clamp installed.

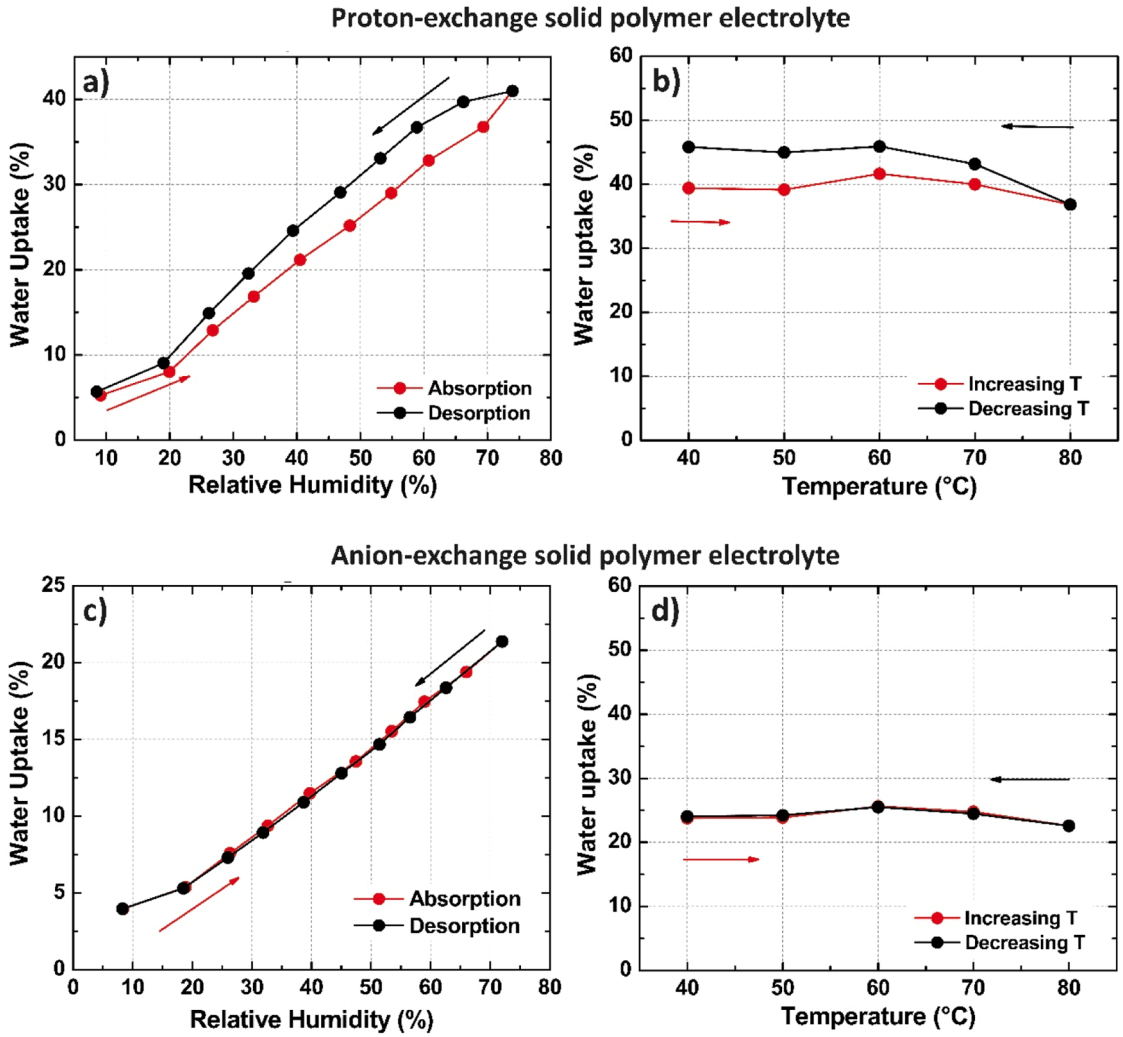

Fig. 4. Water uptake of solid polymer electrolytes in powder form obtained by DVS: a) WU of proton-exchange solid polymer electrolyte powder (SPEP-H^+) at fixed temperature 80 °C; b) WU of SPEP-H^+ at fixed RH (76.9 ± 2.1 °C); c) WU of anion-exchange solid polymer electrolyte powder (SPEP-Cl^-) at fixed temperature 80 °C; d) WU of SPEP-Cl^- at fixed RH (76.4 ± 2.5 °C). Recorded RHs of **b** and **d** can be found in Table S1.

by maintaining a constant RH (see Table S1 for recorded RHs) and increasing or decreasing the temperature of the cell from 40 to 80 °C or 80 °C to 40 °C over 10 °C step intervals. The changes in WU during temperature variation (shown in Fig. 4) of both SPEP-Cl^- and SPEP-H^+ are negligible, suggesting that the influence of relative humidity is much stronger than the influence of temperature, which later with observed dependencies will suggest a kinetic nature of the SPE's conductivities [23,30].

Thermal gravimetric analyzes of both powders were conducted up to 700 °C to verify the thermal stability of the materials at the operating temperatures applied in this work. Fig. S2 evidences a mass loss step starting below 100 °C due to loss of residual water content and/or solvents for both SPEPs. For SPEP-Cl^- there is a three-stage weight loss, indicating degradation of quaternary ammonium groups, followed by degradation of vinylbenzyl chloride grafts, and, lastly, degradation of the polymer backbone [12]. The first degradation step initiates at 180 °C, indicating short-term thermal stability up to this temperature. SPEP-H^+ undergoes degradation in two steps, corresponding to desulfonation and decomposition of the polyphenylene backbone [31,32]. This material shows good thermal stability up to 220 °C.

3.2. Conductivity of SPEs powders evaluated via conventional conductivity cell

Through-plane conductivity measurements in a conventional in-house fabricated conductivity cell (Section 2.4.1) were performed for both types of powders to be used as a comparative basis for the new methodology introduced by Section 2.4.2. Fig. S3 shows examples of impedance spectra for the SPEP-H^+ material at 95 % RH and varying the temperature and for the SPEP-Cl^- at 80 °C and varying relative humidity. The cell containing the SPE powder exhibits a high-frequency semi-circular arc which is typical of an equivalent circuit comprising a parallel combination of bulk resistance and bulk capacitance [33]. Diffusion-limited processes can also be seen in the low-frequency range. Fig. S4 depicts the resulting fitting using a simple Randles equivalent circuit. The impedance of the cell hardware does not need to be included in the circuit since the cell is calibrated by shorting before use and the impedance of the electrodes is automatically subtracted from the measured value. The ionic conductivity of SPE powders was calculated by Eq. (3) using the high-frequency resistance values obtained from the fitting of the impedance spectra.

For the SPEP-H^+, determining the ionic conductivity values under absorption cycles starting from a dry powder was not possible. The stainless steel rods of the cell were designed to have a loose fit with the glass compartment to permit equilibration of the material to the desired

condition during water absorption. However, the water uptaken by the material caused the sample to undergo dimensional swelling, resulting in the disintegration of the pellet and making the powder seep through the cell, which compromised the contact between Pt electrodes and steel rods. To solve this issue, the SPEP-H^+ sample was measured only during desorption, as shown in Fig. 5a. For this measurement, a drop of water was added to the powder before compression. Thus, the compressed material was fully humidified, and the thickness of the water-saturated pellet was used to calculate the conductivity. For SPEP-H^+ it was only possible to measure resistance values at 95 %, 90 %, and 80 % RH in the environmental chamber. For RH < 80 % a loss of contact between the powder and the electrodes was observed due to the increased loss of water and consequent shrinkage of the pellet. The conductivity measured at 80 °C, immediately after cell assembly, was 130 mS cm^{-1} and was identical to that measured after 24 h of equilibration at 95 % RH. This suggests that the values measured at different temperatures at 95 % RH should be considered as conductivity values under fully humidified conditions, Fig. 5b, because a drop of liquid water was added. The obtained value at 80 °C is similar to that previously measured by the group using the same confinement (136 ± 8 mS cm^{-1}) [14].

For the SPEP-Cl^-, it was possible to measure the conductivity during the absorption and desorption of water starting from the dry sample. As observed by the DVS analysis, the anionic SPE possessed half the water uptake at its peak in comparison to SPEP-H^+, thus the measurement was less affected by the dimensional swelling. Fig. 5c shows an exponential increase of the ionic conductivity with increasing RH. At 50 % RH, the conductivity is approximately 1.5 mS cm^{-1} in its chloride form and reaches 24 mS cm^{-1} at 95 % RH. During desorption, there is likely a gradual loss of contact between the pellet and electrodes since the resistance increases step-by-step at each point and nulls at 60 % RH. The volume of the compacted material decreases during desorption and, as the compression between the electrodes is not constant, it results in a loss of contact. Under fully humidified conditions (after adding a drop of liquid water to the powder) the conductivity of the sample increases to 41 mS cm^{-1} at 80 °C. Fig. 5d depicts the conductivity-temperature dependence at 95 %RH (reached from the dry powder) and at full humidification.

Through the conductivity measurements of SPEP-$H^+$and SPEP-Cl^- it was confirmed that the geometry of the conventional in-house made glass cell restricts ingress and egress of water vapor to the powder, causing equilibration of the cell in the humidity chamber to take an unreasonably long time. Moreover, this configuration uses thin Pt disks that tip stainless steel rods which may contribute to contact issues between components.

3.3. Conductivity of SPE powders using the MTS-740 cell

As observed in the previous section, the in-house fabricated through-plane conductivity cell has disadvantages that render it difficult to accurately report the conductivity of SPEs in powder form. The MTS-740

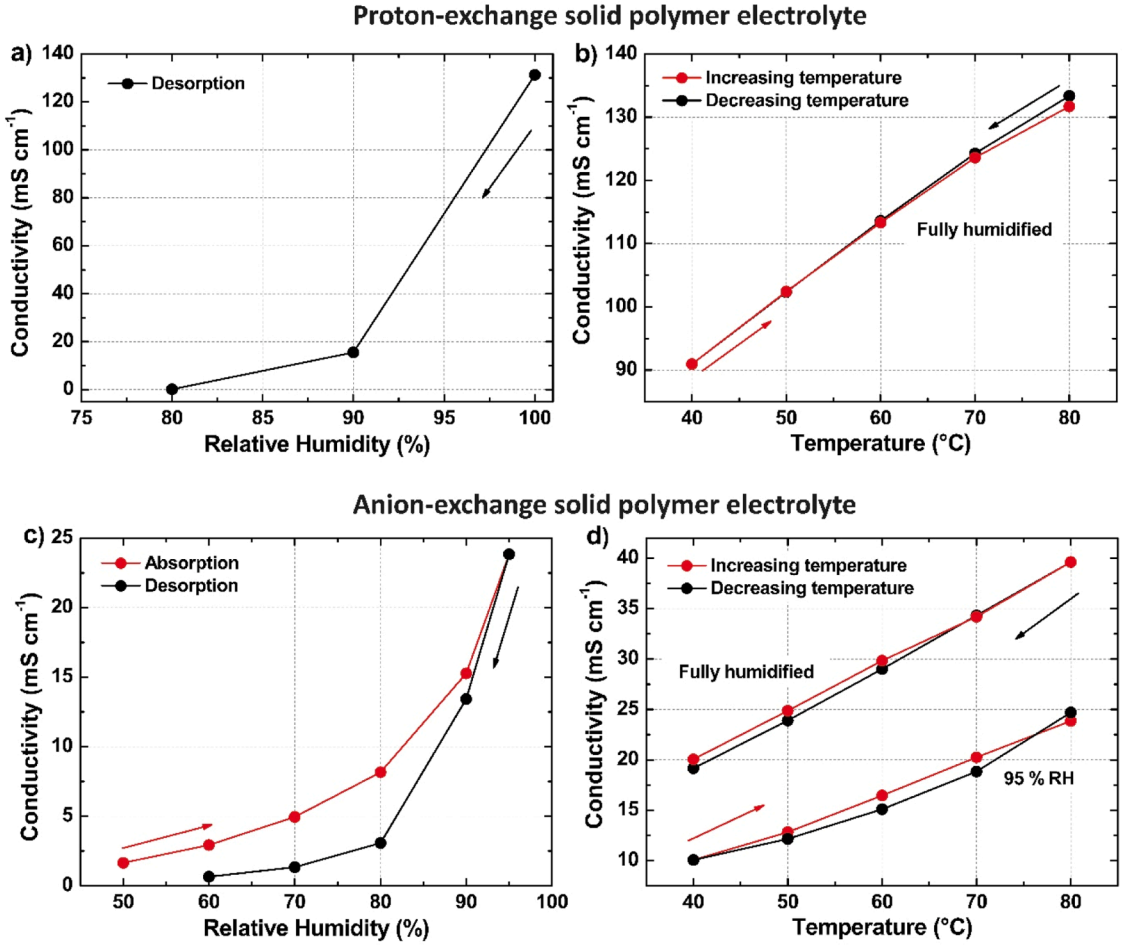

Fig. 5. Ionic conductivity of the solid polymer electrolytes in powder form measured in the conventional in-house made through-plane glass cell: a) RH dependence of the ionic conductivity of proton-exchange solid polymer electrolyte powder (SPEP-H^+) at 80 °C during desorption; b) temperature dependence of the ionic conductivity of fully humidified SPEP-H^+; c) RH dependence of the ionic conductivity of anion-exchange solid polymer electrolyte powder (SPEP-Cl^-) at 80 °C during absorption (red) and desorption (black); d) temperature dependence of the ionic conductivity of fully humidified SPEP-Cl^- and at 95 % RH (starting from dry material).

instrument demonstrated in the past to yield ion conductivity of thin films and is now presented as a solution for accurate measurements of SPEs in their powder form. The measurement steps include the preparation of a powder pellet, through-plane cell assembly, and the analysis of the system's impedance. Each of these steps is discussed separately below.

3.3.1. Pellet characteristics

The preparation of pellets from SPE powders depends on the intrinsic properties of each material. To obtain a fine powder of polymer it is advised to subject it to a milling process (ball-milling, cryo-milling). For each type of polymer, it is necessary to evaluate the optimum pressure for powder compression and the suitable thickness to produce a uniform and free-standing pellet.

In this work, for the SPEP-H^+ material, pellets with thicknesses of ~ 0.5, 1.0, and 1.3 mm were prepared. Pellets with thicknesses < 0.5 mm were increasingly brittle and hard to handle. In addition, for thicker samples, small inconsistencies in the thickness of a pellet are less profound and have a smaller influence on the accuracy of the conductivity value. However, pellets thicker than 1.3 mm require prolonged conditioning time, as they take longer to reach equilibrium upon exposure to water vapor. Moreover, excessively thick samples are prone to form cracks and lose material during the measurement due to decrease in mechanical integrity. In this context, for the SPEP-H^+, the optimized thickness of the pellet was ~ 1 mm. The conditions of optimal compression (pressure and time) for the sample fabrication were determined. Initially, 0.45-ton compression for 2 min was used but a loss of electric contact was observed during the experiment indicating a loss of material inside the conductivity cell due to pellet disintegration. The optimal pellet compression was found to be 0.45-ton for 10 min. In the case of the SPEP-Cl^-, due to the nature of the polymer, higher pressure at a prolonged exposure was necessary to form a mechanically robust pellet. A pressure of 3.0 tons was applied for 10 min to obtain pellets with optimized working thicknesses between 1.3- and 1.5-mm. Pellets with a thickness < 1 mm were difficult to handle and broke easily. For SPEP-Cl^-, to complete a cycle of absorption/desorption, it was necessary to use two different pellets to guarantee the mechanical integrity of the sample during the measurement. For this material, the pellet remained more fragile even in the optimized working thickness. The differences observed between SPEP-$H^+$and SPEP-Cl^- pellets reveal that the intrinsic properties of each polymer powder are important for fabricating a workable pellet for the conductivity measurement.

3.3.2. Assembly of pellet in the through-plane MTS-740 cell

The compressed powder pellet was placed in the through-plane conductivity cell of MTS-740 equipment between the two rectangular platinum electrodes and small round sensing electrodes, as illustrated in Fig. 3. The distance between the electrodes was determined by the thickness of the pellet. The geometry of the system allows microscopic changes in thickness due to the dimensional swelling of the material. Therefore, it was necessary to record the thickness of the pellet after the measurement and applying humidification, when the sample is swollen. If the SPE powder is prone to a high-water uptake, the pellet itself may undergo excessive swelling resulting in a loss of mechanical integrity. Thus, powder spillage into the MTS humidity chamber may occur, even with the designed shields on the sides of the cell. In this case, it is not recommended to exceed 90 % RH during the measurements. For the SPE powders used in this work, it was possible to maintain the pellets at 95 % RH, but at this humidification the samples become fragile and prone to disintegration.

3.3.3. Conductivity measurements

The conductivity value obtained is influenced by both the technique employed and the geometry of the conductivity cell [33]. During in-plane conductivity measurements, the main contribution to the resistance of the system is from the bulk of the material, while other resistances are negligible [34]. This is because of the large cell constant (L/A), Eq. (3), where L is the distance between the electrodes and A is the cross-section of the sample area, which results in high resistance. On the other hand, in through-plane measurements, L corresponds to the thickness of the material and A is the area of the electrodes, which is usually much larger than the first. Therefore, for the through-plane configuration, the magnitude of the material's resistance is small, and contributions of contact and electrode resistance, and electrode-electrolyte interfacial impedance are exacerbated and often observed [35].

In a conventional two-electrode cell configuration for measuring through-plane conductivity, the current source-drain electrodes also serve as voltage-measuring probes. In this case, the contact resistance and lead-wire resistance may be on the order of or exceed the electrolyte resistance [33]. Additionally, charge transfer resistance and electrical double-layer capacitance at the electrode-electrolyte interface can interfere with the measurement and introduce artifacts to the results. In contrast, for the four-probe cell configuration, the voltage- measuring probes are connected through a high-impedance voltmeter so that negligible current flows across these interfaces, thus removing non-linear electrode contributions [19]. Through-plane measurements are commonly performed using a two-terminal configuration due to the fact that placing independent voltage-sense electrodes in a thin ionically conductive phase is challenging, and the results open to broad interpretation. In this context, the MTS-740 system introduced a reliable through-plane method for measuring the resistance of thin materials using a four-terminal configuration (Kelvin connection) [35–37].

Fig. 6 shows Nyquist plots of a) SPEP-H^+ at ~ 95 % RH for different cell temperatures, and b) SPEP-Cl^- pellets at 80 °C under different relative humidities in the MTS-740 equipment. As can be seen, the low and high-frequency impedances exhibit humidity or temperature dependence. The low-frequency impedance is the sum of the ohmic resistance and the charge-transfer impedance of the electrodes [36]. The high-frequency region is the portion of the spectra where the SPE pellet resistance contributions are found. There is no apparent evidence of mass transport impedance in Fig. 6a, but it appears in Fig. 6b for low frequencies. Additionally, in Fig. 6b it is possible to observe the presence of two semicircles, while in Fig. 6a only the second of the two is present. The resolution of the first semicircle depends on the characteristic peak frequency of the given system, which is a function of the dielectric relaxation time of the material [34]. The characteristic peak frequency (ω_p) depends on the bulk resistance of the polymer (R_b) and the bulk capacitance (C_b). R_bC_b is the time constant (τ) or the dielectric relaxation. If the time constant is sufficiently small, little or none of the high-frequency semicircle can be observed in the Nyquist plot [34]. The full semicircle will be obtained only if τ is sufficiently high. The bulk capacitance is dependent on the thickness of the measured material. Thus, it is possible to resolve the semicircles in the high-frequency domain, for example, by increasing the thickness of the SPE pellet. Moreover, the reason for the different spectra for the studied materials is related to the nature of the ion transported. In the case of the SPEP-H^+, the resistance to the conduction of H^+ was measured, while in the case of the SPEP-Cl^-, the resistance is related to the conduction of Cl^-. In water, the ion mobility of protons is ~5 times greater than that of chloride-ions [38], therefore, the resistance to anion transport is expected to be higher. Since the peak frequency depends on the bulk resistance of the SPE, the appearance of a semicircle will also depend on this.

The high-frequency resistance is the sum of a series of ohmic resistances including the SPE's resistance and all non-ionic ohmic contributions. The latter can be gathered into one factor called cell resistance. Cooper [36] has reported the contribution of cell resistance to the MTS-740 system for various thin membranes. For 25 μm thick Nafion 111, the cell resistance was nearly one-fifth of the membrane resistance at 20 % RH and approached half its value at high relative humidity. For much thicker Nafion 117, ~ 178 μm thick, the cell resistance was 5 % of the membrane resistance at low RH and only 15 % at 95 % RH. As the

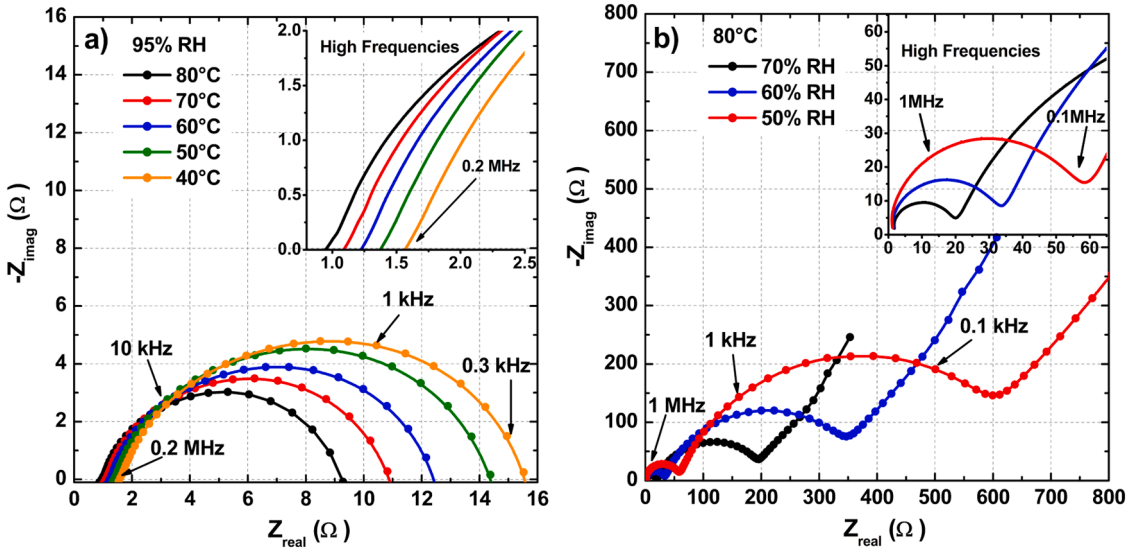

Fig. 6. Nyquist plots of a) proton-exchange solid polymer electrolyte powder (SPEP-H^+) at 95 % RH and different cell temperatures, and b) anion-exchange solid polymer electrolyte powder (SPEP-Cl^-) at 80 °C and different relative humidities. Amplitude 10 mV.

cell resistance is a larger fraction of the membrane resistance for thin membranes than for thick membranes, the cell resistance can then be considered negligible in this present study since the SPE pellets are at least three times thicker than Nafion 117 membranes.

To obtain the ionic resistance of the SPE pellet it is necessary to analyze the impedance spectra to determine the high-frequency resistance. This analysis was performed using least-squares fitting of the impedance spectra data to a Voigt equivalent circuit model as described in the MTS-740 user manual. A series inductor was also included in the equivalent circuit model for better fitting. Fig. S5 shows examples of fittings for SPEP-H^+ and SPEP-Cl^- impedance measurements. The Voigt model is suitable for obtaining the resistance at high frequencies with high accuracy in the MTS-740 cell, even if the semicircle at high frequencies is not present as is the case in Fig. 6a.

With the resistance values obtained through the fitting of the impedance spectrum, the ionic conductivity of the materials under each condition described above was calculated. Fig. 7 depicts the temperature and humidity dependence of the ion conductivity for SPEP-H^+ using three different pellet thicknesses. The profiles of the curves for all three samples are identical. In Figs. 7a, 7c, and 7e, a typical exponential increase of the conductivity with the increase of RH can be seen. However, during desorption, it is possible to observe two different trends: one from 95 % to 80 % RH and another from 70 % to 50 % RH. Desorption from larger pores may be inhibited if they desorb via smaller pores. Therefore, the water loss between 95 % and 80 % RH does not readily occur. When the relative humidity is lowered from 80 % to 70 % RH, the trapped water is released, giving rise to the second portion of the curve. This finding can be better visualized in Fig. S6 which shows the logarithmic plot of Fig. 7g, the average of the three measurements. This graph presents one slope for the absorption curve and two slopes for the desorption curve. The hysteresis effect of the sorption curves is in good agreement with the data collected by DVS measurement, Fig. 4. The higher water uptake in each relative humidity during desorption is compatible with the higher conductivities shown in Figs. 7a, 7c, and 7e (black curves). The obtained conductivities are comparable to similar hydrocarbon-based polymers in membrane form [39].

Figs. 7b, 7d, and 7f show thermally activated behavior of ionic conductivity at ~ 95 % RH (measured RH values for each point can be found in Table S2). The observed hysteresis of the SPEP-H^+ is smaller in the case of the variable temperature. The differences in conductivity between the increasing temperature and decreasing temperature curves seem to be largely influenced by humidity fluctuations at each point caused by the equipment (see Table S2). It is important to note that the conductivity values obtained by the presented method are at least 1.5 times higher than the values collected by the conventional in-house made glass cell (e.g., 210 vs 130 mS cm^{-1}, respectively, at 80 °C). Moreover, limitations of the conventional through-plane glass cell confinement allow measurements only at fully humidified conditions for this polymer, whilst the hardware of the MTS-740 equipment permits reliable data collection at achieved RH at each temperature step. Instrument MTS-740 also allows for the possibility of carrying out high-temperature conductivity measurements by applying backpressure to the system. To verify this, the ionic resistance of SPEP-H^+ was measured at 100 °C and 95 % RH by using 130 kPa of backpressure, resulting in 269 mS cm^{-1} calculated conductivity value.

To confirm the effectiveness of the method for determining the conductivity of anion-exchange SPE powders, the conductivity of the SPEP-Cl^- material was measured, as shown in Fig. 8. The absorption and desorption curves, Fig. 8a, are almost identical and do not exhibit hysteresis. This observation is in agreement with the DVS water sorption/desorption analysis, Fig. 4, which also reveals no hysteresis during this process. Fig. 8b shows the dependence of conductivity on temperature at ~ 95 % RH (measured RH values for each point can be verified at Table S3). A slight difference between the increasing and decreasing temperature curves is observed which may be caused by the fluctuation of RH at each point, as shown in Table S3. The conductivity values of this insoluble polymer powder in the Cl^- form are comparable with the values observed for BTMA radiation-grafted PE-based AEMs in the literature [40,41]. The conductivities presented herein are larger than those measured in the custom-made cell/environmental chamber approach. At 80 °C and 95 % RH, the conductivity determined using the MTS-740 equipment was 53 mS cm^{-1}; in the conventional cell, at the same temperature, the value was 41 and 24 mS cm^{-1} for fully humidified powder and at 95 % RH, respectively.

4. Conclusion

This work demonstrates a precise, simple, and versatile method of measuring the ionic conductivity of emerging ion exchange polymers in their insoluble powder form for advanced energy applications. The results have shown that the fabrication of the solid polymer electrolyte (SPE) powder pellet for the ionic conductivity measurement depends on the intrinsic characteristics of each material and must be adapted for each SPE type. It was possible to measure proton-exchange SPE powder

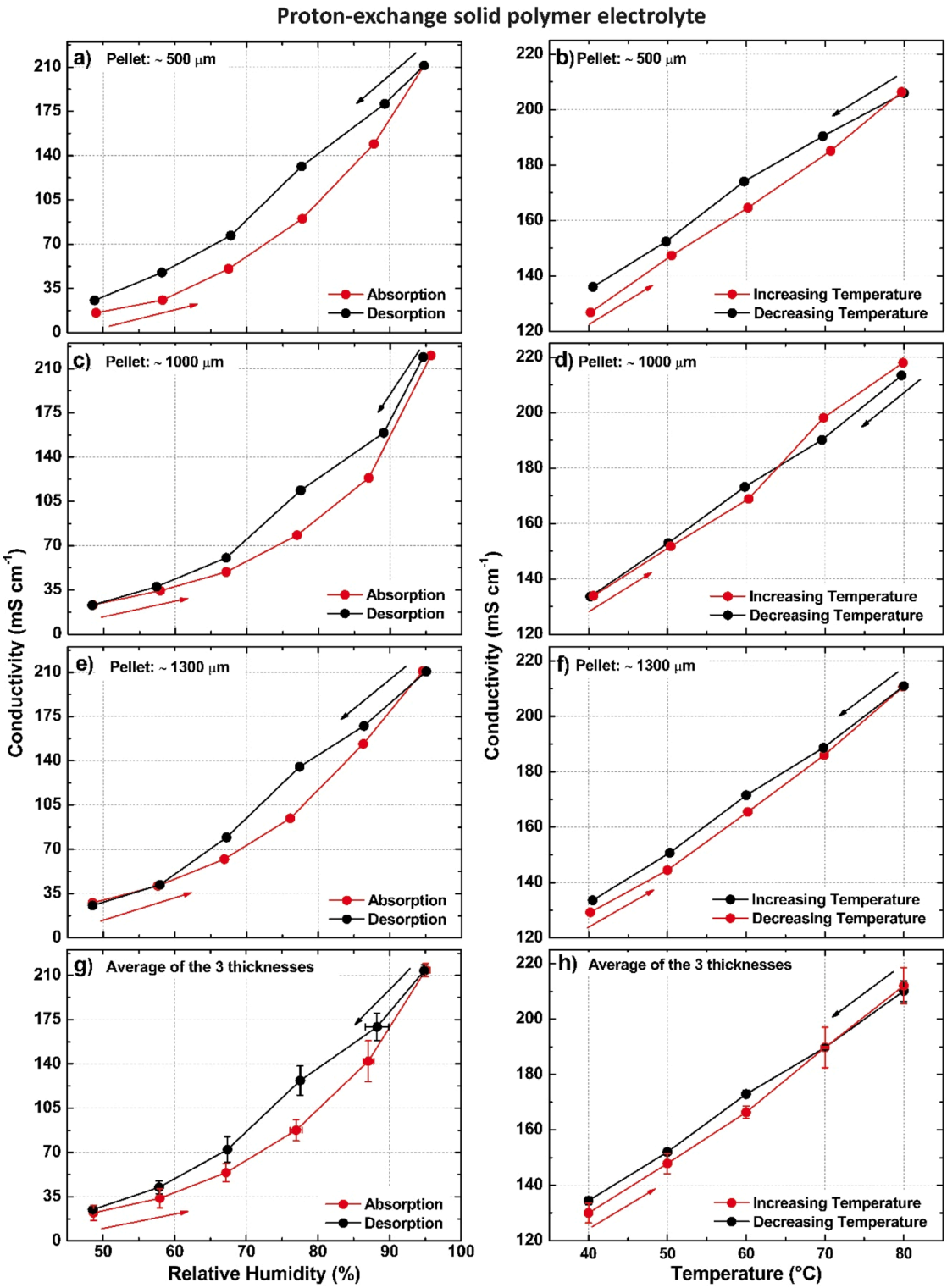

Fig. 7. a, c, and e) Relative humidity dependence of the ionic conductivity of proton-exchange solid polymer electrolyte powder (SPEP-H^+) at 80 °C for pellets with different thicknesses; **b, d, and f)** temperature dependence of the ionic conductivity of SPEP-H^+ at approx. 95 % RH for pellets with different thicknesses; **g)** Average of the 3 thicknesses of relative humidity dependence of the ionic conductivity of SPEP-H^+ at 80 °C; **h)** Average of the 3 thicknesses of temperature dependence of the ionic conductivity of SPEP-H^+ at approx. 95 % RH. Recorded relative humidities of **b, d** and **f** can be found in Table S2.

(SPEP-H^+) pellets having different thicknesses and the obtained conductivity values are consistent through this variation. For this material, the optimized working thickness was found to be ~ 1 mm due to its better mechanical integrity. For the anion-exchange SPE powder (Cl^- form, SPEP-Cl^-), the optimized free-standing pellet was obtained for samples 1.3–1.5 mm thick. The conductivity values gathered by the MTS-740 system were higher than those measured by a conventional through-plane cell; e.g. 210 vs 130 mS cm^{-1}, respectively, for proton-exchange SPE powder at 80 °C and 95 % RH (MTS-740 cell) or fully humidified (conventional glass cell), and 53 vs 24 mS cm^{-1},

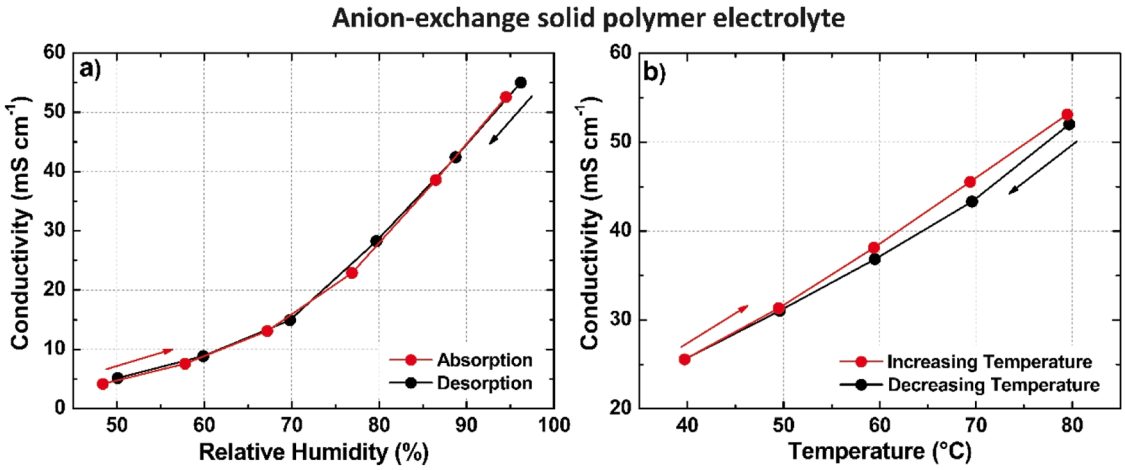

Fig. 8. a) Relative humidity dependence of the ionic conductivity of anion-exchange solid polymer electrolyte powder (SPEP-Cl^-) at 80 °C; **b)** temperature dependence of the ionic conductivity of SPEP-Cl^- at approx. 95 % RH. Recorded relative humidities of **b** can be found in Table S3.

respectively, for anion-exchange SPE powder at 80 °C and 95 % RH (same condition for both cells). These differences are attributed to the geometry of the MTS-740 cell that allows easy access to water vapor, in addition to the four-terminal configuration used for the EIS measurements that provide more accurate results than two-terminal sensing. Moreover, MTS-740 has precise and automated control of chamber temperature and relative humidity. Using the presented new methodology, it was also possible to determine the ionic conductivity value of SPEP-H^+ at 100 °C and 95 % RH by applying 130 kPa of backpressure to the system, which was calculated to be 269 mS cm^{-1}. The demonstrated methodology has therefore proven to be useful in obtaining ionic conductivity of samples for which true conductivity values were inaccessible using other methods.

CRediT authorship contribution statement

A.L.G.B and **A. K.:** Conceptualization, Data curation, Investigation, Methodology, Visualization, Writing – original draft, Writing – review & editing. **E. I. S.:** Writing – review & editing. **S. H.:** Conceptualization, Funding acquisition, Project administration, Resources, Supervision, Writing – original draft, Writing – review & editing.

Declaration of Competing Interest

The authors declare the following financial interests/personal relationships which may be considered as potential competing interests: Steven Holdcroft reports financial support was provided by Natural Sciences and Engineering Research Council of Canada. Ana Laura Goncalves Biancolli reports financial support was provided by State of Sao Paulo Research Foundation. Elisabete Inacio Santiago reports financial support was provided by National Council for Scientific and Technological Development.

Acknowledgments

This work was supported by the Natural Sciences and Engineering Research Council of Canada (NSERC) through Alliance Grant ALLRP 570797 – 21. This work made use of facilities in 4D LABS, SFU. We thank Dr. Simon Cassegrain for providing HB-SPPT SPE powder and members of the Holdcroft Research Group for useful discussions, especially Dr. Torben Saatkamp. ALGB acknowledges FAPESP Grants no. 2019/26955-3 and 2021/14786-2. EIS acknowledges CINE/SHELL (ANP)/FAPESP Grant no. 2017/11937-4 and CNPq 407967/2022-2 for financial support.

Appendix A. Supporting information

Supplementary data associated with this article can be found in the online version at doi:10.1016/j.ijoes.2023.100288.

References

[1] J.A. Turner, A realizable renewable energy future, Handb. Energy Clim. Change 285 (2013) 254–269, https://doi.org/10.4337/9780857933690.00018.
[2] Summary for Policymakers, Global Warming of 1.5 °C, Cambridge University Press, 2022, pp. 1–24, https://doi.org/10.1017/9781009157940.001.
[3] Z.P. Cano, D. Banham, S. Ye, A. Hintennach, J. Lu, M. Fowler, Z. Chen, Batteries and fuel cells for emerging electric vehicle markets, Nat. Energy 3 (2018) 279–289, https://doi.org/10.1038/s41560-018-0108-1.
[4] M. Yue, H. Lambert, E. Pahon, R. Roche, S. Jemei, D. Hissel, Hydrogen energy systems: a critical review of technologies, applications, trends and challenges, Renew. Sustain. Energy Rev. 146 (2021), 111180, https://doi.org/10.1016/j.rser.2021.111180.
[5] Y. Wang, K.S. Chen, J. Mishler, S.C. Cho, X.C. Adroher, A review of polymer electrolyte membrane fuel cells: technology, applications, and needs on fundamental research, Appl. Energy 88 (2011) 981–1007, https://doi.org/10.1016/j.apenergy.2010.09.030.
[6] G. Wu, Current challenge and perspective of PGM-free cathode catalysts for PEM fuel cells, Front. Energy 11 (2017) 286–298, https://doi.org/10.1007/s11708-017-0477-3.
[7] M. Chatenet, B.G. Pollet, D.R. Dekel, F. Dionigi, J. Deseure, P. Millet, R.D. Braatz, M.Z. Bazant, M. Eikerling, I. Staffell, P. Balcombe, Y. Shao-Horn, H. Schäfer, Water electrolysis: from textbook knowledge to the latest scientific strategies and industrial developments, Chem. Soc. Rev. 51 (2022) 4583–4762, https://doi.org/10.1039/d0cs01079k.
[8] D.W. Shin, M.D. Guiver, Y.M. Lee, Hydrocarbon-based polymer electrolyte membranes: importance of morphology on ion transport and membrane stability, Chem. Rev. 117 (2017) 4759–4805, https://doi.org/10.1021/acs.chemrev.6b00586.
[9] M. Adamski, N. Peressin, S. Holdcroft, On the evolution of sulfonated polyphenylenes as proton exchange membranes for fuel cells, Mater. Adv. 2 (2021) 4966–5005, https://doi.org/10.1039/d1ma00511a.
[10] E. Balogun, M. Adamski, S. Holdcroft, Communication—non-fluorous, hydrocarbon PEMFCs, generating > 1 W cm^{-2} power, J. Electrochem. Soc. 167 (2020), 084502, https://doi.org/10.1149/1945-7111/ab88bd.
[11] A.S. Barbosa, A.L.G. Biancolli, A.J.C. Lanfredi, O. Rodrigues, F.C. Fonseca, E. I. Santiago, Enhancing the durability and performance of radiation-induced grafted low-density polyethylene-based anion-exchange membranes by controlling irradiation conditions, J. Membr. Sci. 659 (2022), 120804, https://doi.org/10.1016/j.memsci.2022.120804.
[12] S.D. Poynton, R.C.T.T. Slade, T.J. Omasta, W.E. Mustain, R. Escudero-Cid, P. Ocón, J.R. Varcoe, Preparation of radiation-grafted powders for use as anion exchange ionomers in alkaline polymer electrolyte fuel cells, J. Mater. Chem. A 2 (2014) 5124–5130, https://doi.org/10.1039/c4ta00558a.
[13] A.L. Gonçalves Biancolli, D. Herranz, L. Wang, G. Stehlíková, R. Bance-Soualhi, J. Ponce-González, P. Ocón, E.A. Ticianelli, D.K. Whelligan, J.R. Varcoe, E. I. Santiago, ETFE-based anion-exchange membrane ionomer powders for alkaline membrane fuel cells: a first performance comparison of head-group chemistry, J. Mater. Chem. A 6 (2018) 24330–24341, https://doi.org/10.1039/C8TA08309F.
[14] E. Balogun, S. Cassegrain, P. Mardle, M. Adamski, T. Saatkamp, S. Holdcroft, Nonconformal particles of hyperbranched sulfonated phenylated poly(phenylene) ionomers as proton-conducting pathways in proton exchange membrane fuel cell

catalyst layers, ACS Energy Lett. (2022) 2070–2078, https://doi.org/10.1021/acsenergylett.2c01038.
[15] C. He, A.C. Yang-Neyerlin, B.S. Pivovar, Probing anion exchange membrane fuel cell cathodes by varying electrocatalysts and electrode processing, J. Electrochem. Soc. 169 (2022), 024507, https://doi.org/10.1149/1945-7111/ac4daa.
[16] M. Singh, D. Zappa, E. Comini, Solid oxide fuel cell: decade of progress, future perspectives and challenges, Int. J. Hydrog. Energy 46 (2021) 27643–27674, https://doi.org/10.1016/j.ijhydene.2021.06.020.
[17] D. Pantea, H. Darmstadt, S. Kaliaguine, C. Roy, Electrical conductivity of conductive carbon blacks: influence of surface chemistry and topology, Appl. Surf. Sci. 217 (2003) 181–193, https://doi.org/10.1016/S0169-4332(03)00550-6.
[18] M. Cronau, M. Szabo, C. König, T.B. Wassermann, B. Roling, How to measure a reliable ionic conductivity? The stack pressure dilemma of microcrystalline sulfide-based solid electrolytes, ACS Energy Lett. 6 (2021) 3072–3077, https://doi.org/10.1021/acsenergylett.1c01299.
[19] P. Vadhva, J. Hu, M.J. Johnson, R. Stocker, M. Braglia, D.J.L. Brett, A.J.E. Rettie, Electrochemical impedance spectroscopy for all-solid-state batteries: theory, methods and future outlook, ChemElectroChem 8 (2021) 1930–1947, https://doi.org/10.1002/celc.202100108.
[20] J.C. Douglin, J.R. Varcoe, D.R. Dekel, A high-temperature anion-exchange membrane fuel cell, J. Power Sources Adv. 5 (2020), 100023, https://doi.org/10.1016/j.powera.2020.100023.
[21] J.C. Douglin, R.K. Singh, S. Haj-Bsoul, S. Li, J. Biemolt, N. Yan, J.R. Varcoe, G. Rothenberg, D.R. Dekel, A high-temperature anion-exchange membrane fuel cell with a critical raw material-free cathode, Chem. Eng. J. Adv. 8 (2021), 100153, https://doi.org/10.1016/j.ceja.2021.100153.
[22] K. Yassin, I.G. Rasin, S. Willdorf-Cohen, C.E. Diesendruck, S. Brandon, D.R. Dekel, A surprising relation between operating temperature and stability of anion exchange membrane fuel cells, J. Power Sources Adv. 11 (2021), 100066, https://doi.org/10.1016/j.powera.2021.100066.
[23] M.G. Marino, J.P. Melchior, A. Wohlfarth, K.D. Kreuer, Hydroxide, halide and water transport in a model anion exchange membrane, J. Membr. Sci. 464 (2014) 61–71, https://doi.org/10.1016/j.memsci.2014.04.003.
[24] G.M. Wu, S.J. Lin, C.C. Yang, Preparation and characterization of PVA/PAA membranes for solid polymer electrolytes, J. Membr. Sci. 275 (2006) 127–133, https://doi.org/10.1016/j.memsci.2005.09.012.
[25] C.C. Yang, S.J. Lin, Alkaline composite PEO-PVA-glass-fibre-mat polymer electrolyte for Zn-air battery, J. Power Sources 112 (2002) 497–503, https://doi.org/10.1016/S0378-7753(02)00438-X.
[26] E. Barsoukov, J.R. Macdonald (Eds.), Impedance spectroscopy theory, Experiment, and Applications, Second, JOHN WILEY & SONS INC., Hoboken, New Jersey, 2005.
[27] C. Chen, Y.L.S. Tse, G.E. Lindberg, C. Knight, G.A. Voth, Hydroxide solvation and transport in anion exchange membranes, J. Am. Chem. Soc. 138 (2016) 991–1000, https://doi.org/10.1021/jacs.5b11951.
[28] M. Mandal, G. Huang, N.U. Hassan, X. Peng, T. Gu, A.H. Brooks-Starks, B. Bahar, W.E. Mustain, P.A. Kohl, The importance of water transport in high conductivity and high-power alkaline fuel cells, J. Electrochem. Soc. 167 (2020), 054501, https://doi.org/10.1149/2.0022005jes.
[29] D.S. Kim, C. Welch, R.P. Hjelm, Y.S. Kim, M.D. Guiver, Polymers in Membrane Electrode Assemblies, Elsevier B.V., 2012, https://doi.org/10.1016/B978-0-444-53349-4.00287-9.
[30] K.D. Kreuer, On the complexity of proton conduction phenomena, Solid State Ionics 136–137 (2000) 149–160.
[31] S. Xu, M. Adamski, M. Killer, E.M. Schibli, B.J. Frisken, S. Holdcroft, Sulfophenylated polyphenylenes containing sterically hindered pyridines, Macromolecules 52 (2019) 2548–2559, https://doi.org/10.1021/acs.macromol.8b02289.
[32] M. Adamski, T.J.G. Skalski, B. Britton, T.J. Peckham, L. Metzler, S. Holdcroft, Highly stable, low gas crossover, proton-conducting phenylated polyphenylenes, Angew. Chem. - Int. Ed. 56 (2017) 9058–9061, https://doi.org/10.1002/anie.201703916.
[33] Z. Xie, C. Song, B. Andreaus, T. Navessin, Z. Shi, J. Zhang, S. Holdcroft, Discrepancies in the measurement of ionic conductivity of PEMs using two- and four-probe AC impedance spectroscopy, J. Electrochem. Soc. 153 (2006), E173, https://doi.org/10.1149/1.2258091.
[34] T. Soboleva, Z. Xie, Z. Shi, E. Tsang, T. Navessin, S. Holdcroft, Investigation of the through-plane impedance technique for evaluation of anisotropy of proton conducting polymer membranes, J. Electroanal. Chem. 622 (2008) 145–152, https://doi.org/10.1016/j.jelechem.2008.05.017.
[35] K. Cooper, Characterizing through-plane and in-plane ionic conductivity of polymer electrolyte membranes, ECS Trans. 41 (2011) 1371–1380, https://doi.org/10.1149/1.3635668.
[36] K.R. Cooper, Progress toward accurate through-plane ion transport resistance measurement of thin solid electrolytes, J. Electrochem. Soc. 157 (2010) B1731, https://doi.org/10.1149/1.3481561.
[37] K.R. Cooper, L.L. Scribner, Electrolyte measurement device and measurement procedure, US 7,652,479 B2, Jan. 26, 2010.
[38] J.R. Varcoe, P. Atanassov, D.R. Dekel, A.M. Herring, M.A. Hickner, P.A. Kohl, A. R. Kucernak, W.E. Mustain, K. Nijmeijer, K. Scott, T. Xu, L. Zhuang, Anion-exchange membranes in electrochemical energy systems, Energy Environ. Sci. 7 (2014) 3135–3191, https://doi.org/10.1039/c4ee01303d.
[39] T.J.G. Skalski, M. Adamski, B. Britton, E.M. Schibli, T.J. Peckham, T. Weissbach, T. Moshisuki, S. Lyonnard, B.J. Frisken, S. Holdcroft, Sulfophenylated terphenylene copolymer membranes and ionomers, ChemSusChem 11 (2018) 4033–4043, https://doi.org/10.1002/cssc.201801965.
[40] A.L.G. Biancolli, A.S. Barbosa, Y. Kodama, R.R. de Sousa, A.J.C. Lanfredi, F. C. Fonseca, J.F.Q. Rey, E.I. Santiago, Unveiling the influence of radiation-induced grafting methods on the properties of polyethylene-based anion-exchange membranes for alkaline fuel cells, J. Power Sources 512 (2021), https://doi.org/10.1016/j.jpowsour.2021.230484.
[41] L. Wang, M. Bellini, H.A. Miller, J.R. Varcoe, A high conductivity ultrathin anion-exchange membrane with 500 + h alkali stability for use in alkaline membrane fuel cells that can achieve 2 W cm^{-2} at 80 °C, J. Mater. Chem. A 6 (2018) 15404–15412, https://doi.org/10.1039/c8ta04783a.